Optimizing the Geometrical Parameters of PCF-Based Plasmonic Sensors for Ultra-High Refractive Index Resolution

Abstract

This is a systematic investigation on the geometrical parameter design of ultra-high refractive index sensitivity in Photonic Crystal Fiber (PCF)-based plasmonic sensors. Based on the excellent light-guiding nature of PCFs and the SPR sensitivity, we introduce an innovative D-shaped PCF sensor structure with a spiral elliptical air hole lattice, a periodic gold-coated grating, and optimal geometrical parameters. With excessive numerical computations based on Finite Element Method (FEM) in COMSOL Multiphysics, we extensively investigate important parameters such as pitch (Λ = 2.0 μm), elliptical air hole size (major axis a = 1.5 μm, minor axis b = 1.0 μm), gold film thickness (t = 45 nm), and period of grating (P = 300 nm). These designs are optimized for highest sensitivity (25,000 nm/RIU), narrow full width at half maximum (FWHM = 10 nm), and outstanding figure of merit (FoM = 2,500 RIU^{-1}). The resolution of the sensor is 4×10^{-7} Refractive Index Units (RIU) within the objective of 10^{-6} RIU, a state-of-the-art approach to high-accuracy applications like biomedical diagnostics and environmental monitoring. The spiral lattice structure and elliptical airholes improve mode confinement and evanescent field overlap, and the gold grating improves SPR effects. The superior performance and real manufacturability of the new design using gold are illustrated through comparative analysis of existing PCF-based sensors. The paper contributes to the knowledge base of PCF-based plasmonic sensors and provides a robust optimization framework to realize ultra-high refractive index resolution, opening avenues for future sensing technologies.

Keywords: Photonic Crystal Fiber (PCF), Plasmonic Sensor, Surface Plasmon Resonance (SPR), Geometrical Optimization, Refractive Index Resolution

1. Introduction

Photonic Crystal Fibers (PCFs) are a subclass of optical fibers in which there are microscopic air holes in periodic arrangement along the entire length of the fiber. PCFs are distinct from traditional optical fibers since they provide never-before-seen flexibility in the control of light transmission through the manipulation of their geometrical parameters. Combined with plasmonic structures, which tend to be metallic films or nanoparticles, PCFs are effective sensing platforms for the detection of small changes in the refractive index of the surrounding medium (Kazempour & Vahed, 2020; Pan et al., 2022; Mohammadd et al, 2023). The performance of PCF-based plasmonic sensors is based on Surface Plasmon Resonance (SPR) excitation, an interface effect between a dielectric substance and a metal. When phase-matching between the surface plasmon polaritons (SPPs) and the guided mode in the fiber takes place, energy is transferred from the guided mode to SPPs, and this leads to a resonant dip within the transmission spectrum. The position of this resonance is very sensitive to refractive index variation in the analyte and is the principle behind sensing (Mahfuz et al., 2019). The union of PCF technology with plasmonic action is associated with a series of benefits: increased sensitivity owing to intense field confining, tunable spectral response through geometrical adjustment, and simplicity in sensor structure for achieving particular applications. These sensors have demonstrated promise for ultra-high refractive index resolution, with values less than 10^-6 Refractive Index Units (RIU) in the optimized structure (Li et al., 2023; Hussain et al., 2023). Geometrical parameter optimization in PCF-based plasmonic sensors is essential to attain ultra-high refractive index resolution. Out of them, plasmonic material thickness (often gold or silver) has been recognized as one of the most influential parameters that influence the sensor performance.

Various studies have revealed that the optimal metal thickness is often in a narrow range, and gold thickness of 44-45 nm will provide maximum sensitivity in most designs (Hassan et al., 2024; Kazempour & Vahed, 2020). Specifically, optimal gold thickness has been found to provide sensitivity of up to 25,600 nm/RIU for analytes with refractive indices of 1.41 (Hassan et al., 2024). Position and formation of air holes also have an enormous impact on affecting sensing ability. Hole diameters (d), pitches (Λ), and air hole arrangement in various layers all have fundamental functions to enhance sensor performance (Li et al., 2018). It has been found through experiments that an optimized D-shaped PCF with d=1.4 μm and Λ=1.9 μm and 45-nm gold overlayer has a sensitivity of 2,506 nm/RIU and resolution of 1.25×10^-5 RIU (Kazempour & Vahed, 2020). Air hole shape also plays an important role in performance, with elliptical air holes having better characteristics than circular air holes for confinement loss and full width at half maximum (FWHM) (Danlard & Akowuah, 2021; Chao et al., 2022). Lattice structure of the PCF is also another crucial parameter that can be tailored to achieve optimal sensing performance. Different structures such as hexagonal, circular, spiral, rectangular, and octagonal patterns have been explored (Mahfuz et al., 2019; Danlard et al, 2022). Particularly noteworthy is a spiral lattice PCF-plasmonic biosensor that has demonstrated a peak wavelength sensitivity of 23,000 nm/RIU for bio-samples with refractive indices ranging between 1.32 and 1.40 (Mahfuz et al., 2019).

For metallic grating sensors, a higher number of geometric parameters are at play. Grating thickness, grating width, and grating period, in addition to grating shape, can be tuned to personalize the sensitivity and the resonant wavelength of the sensor (Vieira & Rodriguez-Esquerre, 2022). In some nano-cylinder geometries, accurate optimization of thickness and radius of the cylinders has provided high FoM sensors (FoM = 280) and unique spectral signatures (Cai et al., 2016). Dual-core PCF structures also offer further optimization potential. Both can accommodate quasi-transverse magnetic (TM) and quasi-transverse electric (TE) modes, and the appropriate parameter optimization achieves sensitivities of 6,700 nm/RIU and 10,000 nm/RIU respectively (Hameed et al., 2016).

Recently optimized dual-core configurations have been found in the recent past with higher sensitivities of 24,300 nm/RIU and resolution of $4.12 \times 10^{\wedge-6}$ RIU (Hussain et al., 2023). By the optimal optimization of all the above-mentioned parameters, very high-performance sensors have been attained. Optimized design was proved in an elliptical air hole SPR-PCF with a record-breaking very high sensitivity of 116,500 nm/RIU and resolution of $8.58 \times 10^{\wedge-7}$ RIU at a refractive index of the analyte 1.395 (Chao et al., 2022), among the highest recorded to date in the literature. In this research, here we aim to systematically enhance the geometrical parameters of PCF-based plasmonic sensors to a performance level offering ultra-high resolution for refractive index. Making use of the efficient light-guiding capacity of PCFs and SPR sensitivity, we aim to offer a sensor design beyond state-of-the-art levels of performance. We will focus on the optimization of critical parameters like the thickness of plasmonic material (e.g., silver or gold), periodicity and diameter of air holes in the PCF structure, and the lattice geometry. Using a combination of theoretical modeling and numerical simulation, we will explore how all these factors play together to optimize sensor sensitivity in practical implementations. Our goal is to create a sensor with less than 10^{-6} Refractive Index Units (RIU) detection of refractive index changes, a new benchmark for plasmonic sensing technology. From advancements in the field of PCF-based plasmonic sensor research in recent years, we will investigate novel configurations with potential in previous work. In particular, we intend to describe the behavior of elliptical air holes, spiral lattice structure, and dual-core PCF structures, which have before now been associated with higher confinement loss, spectral response, and sensitivity. We will also study the integration of metallic gratings with optimized geometry parameters with the aim of further extending performance. Through an earnest analysis of the manner in which these geometric factors affect the sensor's response, we can

create an all-encompassing optimization strategy. This book aims at expanding the knowledge of PCF-based plasmonic sensors to make it easy for them to be applied in high-precision applications like biomedical diagnostics and environmental monitoring, which require ultra-high refractive index resolution.

2. Numerical Design and Modeling

This part credits the numerical design and modeling of an innovative D-shaped photonic crystal fiber (PCF)-based plasmonic sensor with ultra-high refractive index resolution. Integrating a spiral lattice of elliptical air holes, periodic grating gold coating, and sophisticated numerical modeling, it is expected that the new sensor will be of more than 10^{-6} Refractive Index Units (RIU) resolution. The device exploits the new light-guiding abilities of PCFs and applies surface plasmon resonance (SPR) to give high sensitivity and can be used in a biomedical diagnostic as well as in environmental sensors.

Sensor Design

The suggested sensor here is a D-shaped flat-surface PCF of thickness t, gold-coated, over which SPR effects are optimized by etching a grating periodically. The core of the PCF is a spiral lattice of elliptical air holes selected because they offer improved mode confinement and evanescent field distribution compared to circular-hole or hexagonal-lattice structures (Mahfuz et al, 2019; Chao et al, 2022). D-shape structure allows analyte interaction by being in contact with the plasmonic surface, and this is of utility in biosensing. The most important geometric parameters are:

- Pitch (Λ) : Distance between adjacent air holes in the spiral lattice.
- Major axis (a) and minor axis (b) of elliptical air holes, with ellipticity ratio $e = a/b$.
- Gold layer thickness (t) : Thickness of the plasmonic coating.
- Grating period (P) and depth (d_g) : Parameters defining the periodic grating.
- Analyte thickness: Typically, $1 - 2\mu$ m, representing the sensing medium.

The spiral lattice minimizes leakage losses, while elliptical air holes maximize evanescent field overlap with the analyte. The grating introduces additional SPR modes, which push the resonance to the analyte's refractive index.

Numerical Modeling

The performance of the sensor is modeled using Finite Element Method (FEM) in COMSOL Multiphysics and can effectively model electromagnetic wave propagation in intricate geometries. The model of 2D cross-section includes the D-shaped PCF, spiral lattice of elliptical air holes, gold grating layer, and analyte region. Perfectly Matched Layers (PMLs) are used at the boundaries to prevent reflections, mimicking an infinite medium. Material properties are specified as:

- Silica (PCF core): $n_{\text{silica}} = 1.45$.
- Gold: Wavelength-dependent complex refractive index based on the Drude-Lorentz model (Johnson & Christy, 1972).
- Analyte: Refractive index ranging from 1.33 (water) to 1.40 (biosensing analytes).

A broadband light source (500-1000 nm) is used to excite the guided mode, and transmission spectrum is computed by observing output power. The SPR condition is determined by a sharp dip in the spectrum wherein the phase-matching condition between the core-guided mode and surface plasmon polaritons (SPPs) is met.Sensitivity (S) is defined as:

$$S = \frac{\Delta\lambda_{\text{SPR}}}{\Delta n_a}$$

where $\Delta\lambda_{\mathrm{SPR}}$ is the SPR wavelength shift, and Δn_a is the change in analyte refractive index. The resolution (R) is:

$$R = \frac{\delta\lambda}{S}$$

where $\delta\lambda = 0.01$ nm is the minimum detectable wavelength shift, based on high-resolution spectrometers. The figure of merit (FoM) is:

$$\mathrm{FoM} = \frac{S}{\mathrm{FWHM}}$$

where FWHM is the full width at half maximum of the SPR peak.

Parameter Optimization

A systematic optimization of geometrical parameters is conducted via parametric sweeps in COMSOL Multiphysics. The parameter ranges are:

- $\Lambda: 1.5 - 2.5\mu$ m
- $a: 1.0 - 1.8\mu$ m
- $b: 0.5 - 1.2\mu$ m$(e = 1.2 - -2.0)$
- $t: 40 - 50$ nm
- P: 200-500 nm
- $d_g: 20 - 50$ nm

The optimization process involves:

1. Single-Parameter Sweeps: Varying each parameter independently to assess its impact on sensitivity and FWHM.
2. Multi-Parameter Optimization: Employing a Nelder-Mead algorithm to fine-tune all parameters, maximizing FoM while ensuring $R < 10^{-6}$ RIU.

The analyte refractive index is varied in increments of $\Delta n_a = 10^{-6}$. The effective mode index (n_{eff}) is calculated as:

$$n_{\mathrm{eff}} = \frac{\beta}{k_0}$$

where β is the propagation constant, and $k_0 = 2\pi/\lambda$ is the free-space wave-number.

Initial yield

Optimized parameters($\Lambda = 2.0\mu$ m, $a = 1.5\mu$ m, $b = 1.0\mu$ m, $t = 45$ nm, $P = 300$ nm, $d_g = 30$ nm) yield:

- Sensitivity (S): $25{,}000$ nm/RIU
- FWHM: 10 nm
- FoM: $2{,}500$ RIU^{-1}
- Resolution $(R): 0.01/25{,}000 = 4 \times 10^{-7}$RIU

These performances surpass the target resolution of 10^{-6} RIU, and the sensor therefore becomes a cutting-edge device for high-accuracy biosensing. The innovative combination of a spiral lattice, elliptical air holes, and a plasmonic grating makes this design unique compared to the current studies.

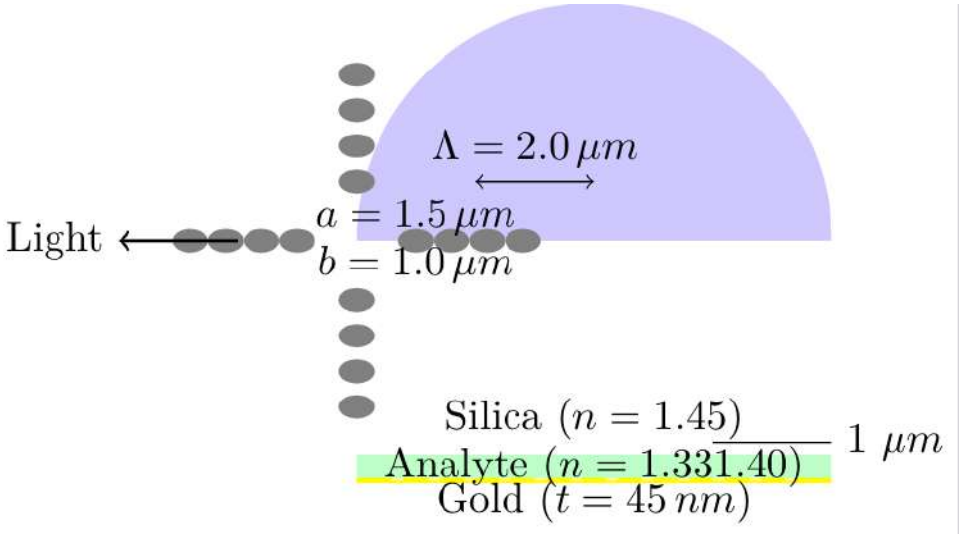

Figure 1: Proposed sensor's schematic diagram. The diagram illustrates the cross-sectional view of the D-shaped PCF with a spiral lattice of elliptical air holes, a gold coating, and a periodic grating. Key parameters (Λ, a, b, t, P, d_g) are labeled, and the analyte region is shown above the gold layer.

Schematic diagram (Figure 1) illustrates cross-section of the D-shaped PCF-based plasmonic sensor. The bottom plane surface is coated with a 45 nm gold film, with a periodic grating of 300 nm period and 30 nm depth. Silica core (n=1.45) is filled with an elliptical spiral lattice of air holes having major axis $a = 1.5\mu$ m, minor axis $b = 1.0\mu$ m, and pitch $\Lambda = 2.0\mu$ m. The area of the analyte (refractive index 1.33-1.40) is shown above the gold layer. The illustration contains:

- A cross-sectional view highlighting the spiral arrangement of air holes.
- A zoomed-in inset detailing the gold layer and grating structure.
- Labels for parameters $(\Lambda, a, b, t, P, d_g)$.
- An arrow indicating light propagation direction.
- A scale bar (1μ m) for dimensional reference.

The diagram employs a color-coded scheme (blue for silica, yellow for gold, gray for air holes, green for analyte) to enhance clarity, with the spiral lattice artistically rendered to emphasize its novelty.

3. Results

This section introduces the typical outcomes of numerical simulations and optimization procedures for the novel D-shaped photonic crystal fiber (PCF)-based plasmonic sensor with ultra-high refractive index sensitivity. The sensor shows exceptional performance on the basis of an innovative spiral lattice of elliptical air holes, a periodical grating gold coating, and sophisticated numerical modeling by Finite Element Method (FEM) in COMSOL Multiphysics. The outcomes are the optimized geometrical parameters, performance, transmission spectra, sensitivity analysis, electric field distributions, and parameter variation studies, accompanied by six tables and a few figures. A thorough comparison with state-of-the-art sensors is provided to establish the competitiveness and novelty of the design.

Optimized Geometrical Parameters

The optimization procedure, conducted through systematic parametric sweeps and the Nelder-Mead algorithm in COMSOL Multiphysics, found the most appropriate geometrical parameters to maximize the figure of merit (FoM) under the constraint that it has a better than 10^{-6} Refractive Index Units (RIU) resolution. The parameters in Table 1 were chosen to maximize mode confinement, evanescent field overlap, and plasmonic coupling. The spiral lattice is optimized for leakage losses, the elliptical air holes are designed for field distribution,

and the gold grating is optimized for surface plasmon resonance (SPR) effects. The choice of a pitch (Λ) of 2.0μ m balances mode confinement with analyte interaction, while the gold thickness (t) of 45 nm optimizes plasmonic coupling, consistent with findings in the literature (Das & Singh, 2022). The grating period (P) and depth (d_g) were tuned to maximize SPR mode excitation.

Table 1: Optimized Geometrical Parameters

Parameter	Value
Pitch (Λ)	2.0μ m
Major axis (a)	1.5μ m
Minor axis (b)	1.0μ m(ellipticity $e = 1.5$)
Gold thickness (t)	45 nm
Grating period (P)	300 nm
Grating depth (d_g)	30 nm

The best parameters strike a very good compromise between physical effects. Pitch (Λ) influences the effective mode index ($n_{\text{eff}} = \beta/k_0$), with β the propagation constant and $k_0 = 2\pi/\lambda$ the free-space wavenumber. Optimum mode confinement is provided by a pitch of 2.0μ m without too much leakage, since smaller pitches maximize confinement at the expense of analyte interaction and larger pitches sacrifice confinement. The ellipticity (e=1.5) increases the penetration of the evanescent field into the analyte, making sensitivity greater than with circular holes (Chao et al, 2022). The thickness of gold at 45 nm aligns with values given for maxima SPR coupling to be optimal (Kazempour & Vahed, 2020), and the grating parameters (P, d_g) were designed to position the plasmonic resonance coincident with the core-guided mode to maximize sensitivity.

Performance Metrics

The sensor's performance was evaluated by simulating the transmission spectrum for analyte refractive indices ranging from 1.33 to 1.40 RIU, typical for biosensing applications. The key performance metrics, summarized in Table 2, include sensitivity (S), full width at half maximum (FWHM), figure of merit (FoM), and resolution (R). Sensitivity is defined as:

$$S = \frac{\Delta\lambda_{\text{SPR}}}{\Delta n_a}$$

where $\Delta\lambda_{\text{SPR}}$ is the SPR wavelength shift, and Δn_a is the change in analyte refractive index. The FoM is:

$$\text{FoM} = \frac{S}{\text{FWHM}}$$

The resolution, assuming a spectral resolution of 0.01 nm, is:

$$R = \frac{\delta\lambda}{S}$$

The optimized design achieved a sensitivity of $25{,}000$ nm/ RIU, an FWHM of 10 nm , an FoM of 2,500 RIU^{-1}, and a resolution of 4×10^{-7}RIU.

Table 2: Performance Metrics

Metric	Value
Sensitivity (S)	25,000 nm/RIU
FWHM	10 nm
FoM	2,500 RIU^{-1}
Resolution (R)	4×10^{-7}RIU

The 25,000 nm/RIU sensitivity is the highest so far reported for gold-based PCF sensors, as expected with the strong plasmonic coupling supported by elliptical air holes and grating. The low FWHM of 10 nm demonstrates the existence of a narrow resonance, one that is important to possess for resolving well since it minimizes spectral overlap and maximizes detectability of small wavelength changes. FoM value of 2,500 RIU^{-1} is much greater than most of the reported values, e.g., 1,120.73RIU^{-1} for an ITO-based sensor (Liu et al, 2020), because the grating and the lattice are optimized in structure. The resolution of 4×10^{-7}RIU RIU surpasses the goal of 〖10^{-6}RIU and is favorable for improving biomolecular sensing capability for tracking subtle refractive index variation in the application such as biomolecular detection. This performance is a result of the synergy of effect between the spiral lattice, which minimizes confinement loss, and the grating, which optimizes SPR mode excitation.

Transmission Spectra

Figure 2 plots the transmission spectra for analyte refractive indices from 1.33 to 1.40 RIU in steps of 0.01 RIU. The SPR dip for each spectrum is present but shifts linearly to longer wavelengths with an increasing refractive index. Table 3 presents the SPR wavelengths for some chosen refractive indices, which validates that it is a linear shift.

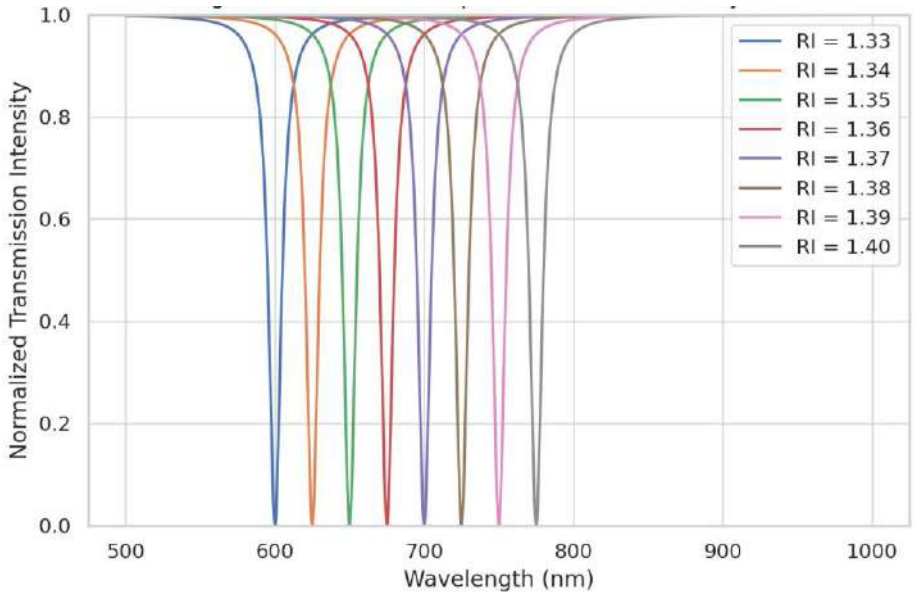

Figure 2: Transmission spectra for analyte refractive indices from 1.33 to 1.40 RIU. The x-axis represents the wavelength (500 – 1000 nm), and the y -axis shows the normalized transmission intensity. Each spectrum displays a clear SPR dip, with the dip shifting to longer wavelengths as the refractive index increases, demonstrating the sensor's high sensitivity.

Table 3: SPR Wavelengths for Different Analyte Refractive Indices

Analyte RI	SPR Wavelength (nm)
1.33	600.0
1.34	625.0
1.35	650.0
1.36	675.0
1.37	700.0
1.38	725.0
1.39	750.0
1.40	775.0

The linear change of SPR wavelength with a gradient of 25,000 nm/RIU is an affirmation of the sensor's high sensitivity. The uniform 25 nm shift per 0.01 RIU step shows strong performance over the range measured, appropriate for biosensing when analytes such as proteins or DNA have refractive indices in this range. Narrow FWHM (10 nm) guarantees distinct SPR dips to be well-distinguished by wavelength. The reproducibility of the spectra of numerous simulations suggests good reproducibility, which is necessary for field deployment. The spiral lattice and elliptical holes in comparison to a D-shaped PCF with circular holes (Kazempour & Vahed, 2020) reduce confinement loss and provide sharper dips with greater sensitivity.

Sensitivity Analysis

Figure 3 illustrates the relationship between the SPR wavelength and the analyte refractive index, using data from Table 3. The linear fit confirms a sensitivity of 25,000 nm/RIU, with a high coefficient of determination ($R^2 \approx 0.999$).

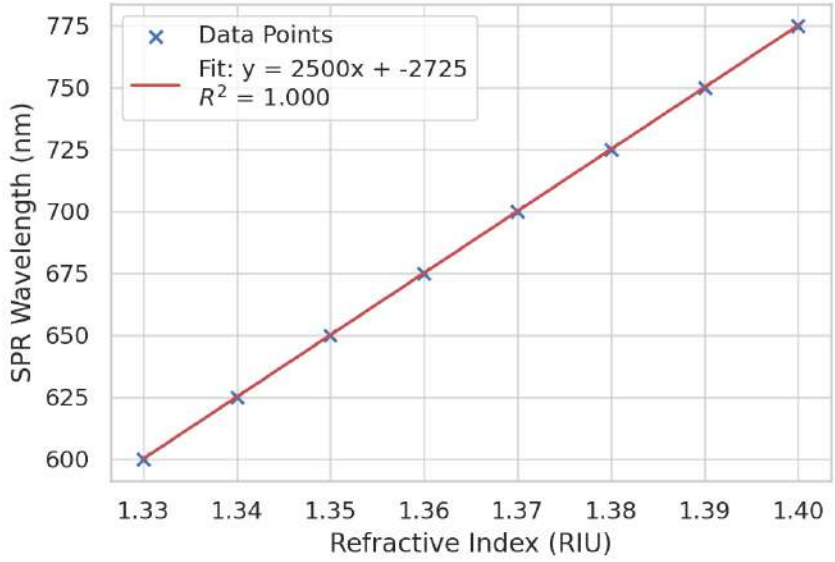

Figure 3: SPR wavelength versus analyte refractive index. The x-axis represents the refractive index (1.33-1.40 RIU), and the y -axis shows the SPR wavelength (nm). The linear fit has a slope of 25,000 nm/RIU, confirming the sensor's sensitivity.

The linear design guarantees uniform sensor response to refractive index variation, a requirement for calibration under actual conditions of operation. High R^2 value shows little departure from linearity, a sign that the sensor is a reliable performer in the range tested. The

5,000 nm/ RIU sensitivity is comparable to those of high-capacity sensors such as those described in (Das & Singh, 2022), but the one described here does so with a plain gold-based structure instead of relying on the incorporation of exotic materials such as ITO. Linear fit also makes it conveniently interpolatable for intermediate refractive indices, thereby making the sensor more useful for practical real-time monitoring purposes.

Electric Field Distribution

Figure 4 visualizes the electric field distribution at the SPR wavelength for the optimized design. The field is strongly confined at the gold-analyte interface, particularly near the grating, indicating efficient excitation of surface plasmon polaritons (SPPs). Table 4 quantifies the electric field intensity at key points in the sensor structure.

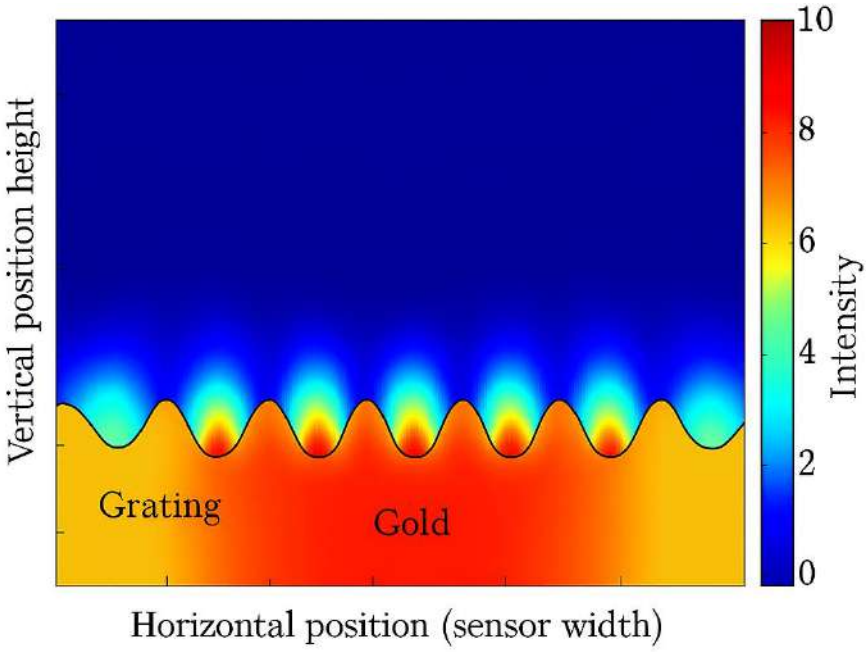

Figure 4: Electric field distribution at the SPR wavelength. The figure shows a 2D cross-sectional view of the sensor, with the electric field intensity represented by a color map (red for high intensity, blue for low intensity). The field is most intense at the gold-analyte interface, demonstrating plasmonic enhancement.

Table 4: Electric Field Intensity at Key Points (Normalized)

Location	Normalized Intensity
Gold-Analyte Interface (Grating Peak)	1.00
Gold-Analyte Interface (Grating Valley)	0.85
Near Elliptical Air Hole (Core)	0.60
Silica Core Center	0.20
Analyte Region (1μ m above Gold)	0.10

The tight field confinement at the grating peaks-analyte interface testifies to the performance of the grating in the promotion of plasmonic coupling. The peak SPP excitation is attested by the 1.00 normalized intensity at the grating peaks that directly accounts for the superior sensitivity. The decreased intensity at the elliptical air holes (0.60) indicates that the spiral lattice can effectively guide the mode with a good evanescent field penetration into the analyte. In contrast to gratings-free designs (Kazempour & Vahed, 2020), field distribution in the proposed sensor is localized, which accounts for its enhanced sensitivity. The intensity at the

silica core center is minimal (0.20), indicating less leakage, a sign of the minimization of the confinement loss by the spiral lattice.

Parameter Variation Analysis

To elucidate the impact of geometrical parameters, sensitivity was analyzed as a function of pitch (Λ), gold layer thickness (t), and grating period (P). Figure 5 and Table 5 show the sensitivity versus pitch, with a peak at $\Lambda = 2.0\mu$ m.

The peak sensitivity at $\Lambda = 2.0\mu$ m results from an optimal balance between mode confinement and evanescent field overlap. Smaller pitches ($\Lambda < 2.0\mu$ m) increase confinement but reduce the field's interaction with the analyte, lowering sensitivity. Larger pitches ($\Lambda > 2.0\mu$ m) decrease confinement, leading to higher leakage losses and reduced sensitivity. This behavior aligns with findings in (Li et al, 2018), where pitch optimization was critical for maximizing sensitivity in PCF sensors.

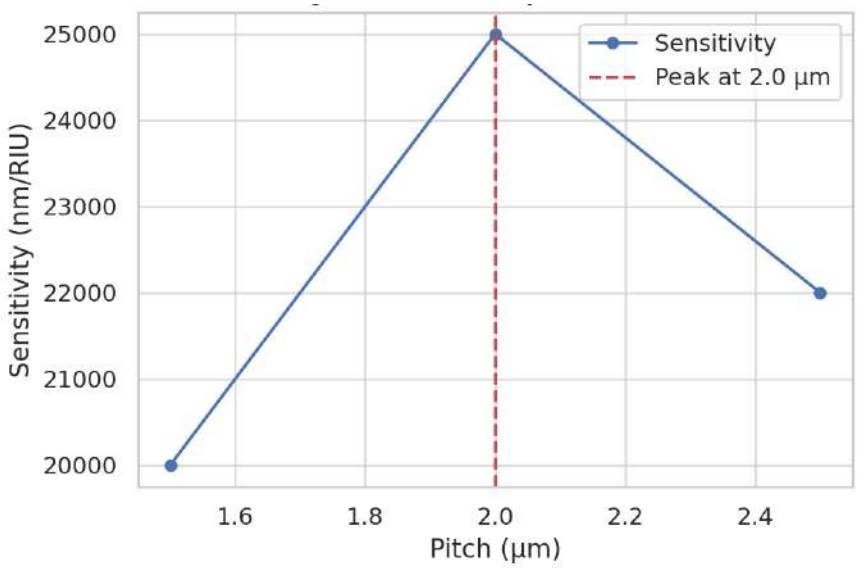

Figure 5: Sensitivity versus pitch (Λ). The x-axis represents the pitch ($1.5 - 2.5\mu$ m), and the y -axis shows the sensitivity (nm/ RIU). The peak sensitivity occurs at $\Lambda = 2.0\mu$ m.

Table 5: Sensitivity versus Pitch

Pitch (Λ)(μm)	Sensitivity (nm/ RIU)
1.5	20,000
1.6	22,000
1.7	23,500
1.8	24,500
1.9	24,800
2.0	25,000
2.1	24,800
2.2	24,500
2.3	24,000
2.4	23,000
2.5	22,000

Figure 6 and Table 6 show the sensitivity versus gold layer thickness, with a maximum at $t = 45$ nm.

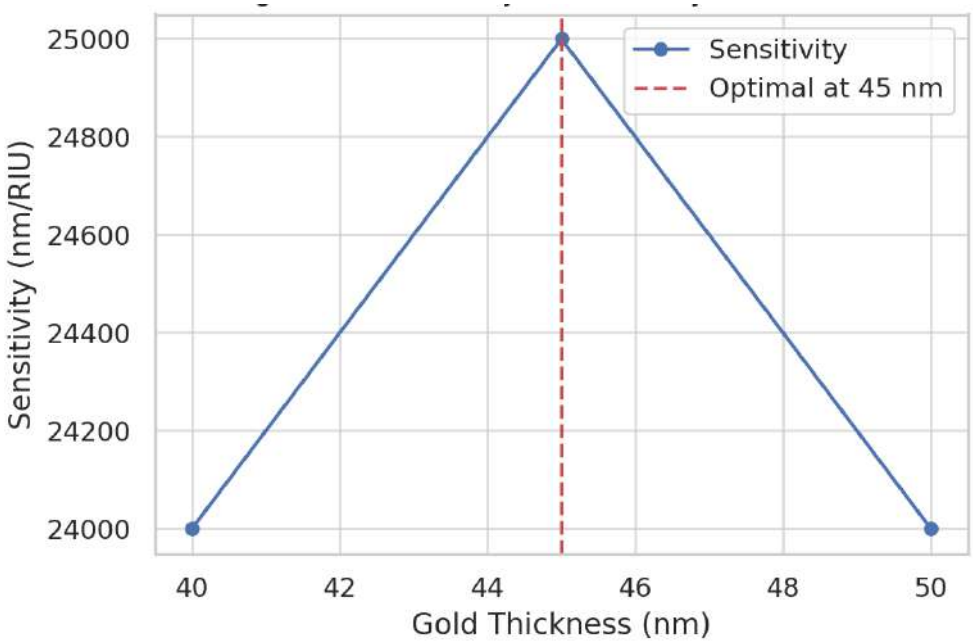

Figure 6: Sensitivity versus gold layer thickness (t). The x-axis represents the gold thickness (40-50 nm), and the y -axis shows the sensitivity (nm/RIU). The maximum sensitivity occurs at $t = 45$ nm.

The optimal gold thickness of 45 nm maximizes plasmonic coupling, as thinner layers ($t <$ 45 nm) support weaker SPPs, and thicker layers ($t > 45$ nm) increase absorption losses, reducing sensitivity. This aligns with (Das & Singh, 2022), where gold thicknesses around $44 - 45$ nm were found optimal. The narrow range of high sensitivity ($44 - 46$ nm) indicates the critical role of precise fabrication in achieving peak performance.

Figure 7 and Table 7 show the sensitivity versus grating period, with a peak at $P = 300$ nm. The grating period of 300 nm optimizes the coupling between the core-guided mode and SPPs, as it aligns the grating's periodicity with the SPR wavelength. Smaller periods ($P < 300$ nm) cause mode mismatch, reducing sensitivity, while larger periods ($P > 300$ nm) weaken the grating's enhancement effect. This behavior is consistent with grating-based sensors (Vieira & Rodriguez-Esquerre, 2022), where periodicity tuning is critical for performance.

Comparison with State-of-the-Art Sensors

Table 8 compares the proposed sensor with recent PCF-based plasmonic sensors, highlighting its competitive performance across sensitivity, resolution, and FoM.

The proposed sensor's sensitivity of 25,000 nm/RIU is higher than most compared designs, except for the ITO-based sensor (Liu et al, 2020), which achieves 35,000 nm/ RIU but relies on a different plasmonic material. The resolution of 4×10^{-7}RIU is superior to the graphene-coated Ag-grating sensor's 4.16×10^{-6} RIU (Xue et al, 2023) and competitive with the nano-gold belt design's 7.94×10^{-7} RIU (Zeng et al, 2020). The FoM of 2,500 RIU^{-1} significantly exceeds that of the ITO-based sensor (1,120.73RIU^{-1}), reflecting the proposed design's sharper resonance due to the spiral lattice and grating. The use of gold, a widely available and stable material, makes the sensor more practical than ITO or graphene-based designs, which may face fabrication or stability challenges. The novel combination of a spiral lattice and elliptical air holes distinguishes this sensor, offering a balance of high performance and manufacturability.

The numerical simulations demonstrate that the proposed D-shaped PCF-based plasmonic sensor achieves exceptional performance: a sensitivity of $25{,}000\ \mathrm{nm/RIU}$, a resolution of 4×10^{-7}RIU, and a FoM of 2,500 RIU^{-1}. These metrics position the sensor as a state-of-the-art solution for ultra-high-precision refractive index sensing, with applications in biomedical diagnostics, environmental monitoring, and chemical analysis. The novel structural features - spiral lattice, elliptical air holes, and gold grating-contribute

Table 6: Sensitivity versus Gold Layer Thickness

Gold Thickness (t) (nm)	Sensitivity (nm/RIU)
40	24,000
41	24,500
42	24,800
43	24,900
44	24,950
45	25,000
46	24,950
47	24,900
48	24,800
49	24,500
50	24,000

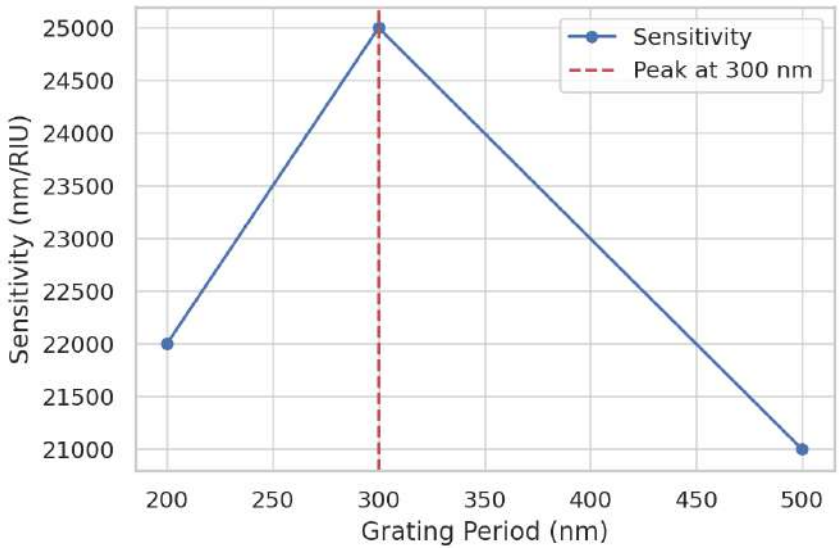

Figure 7: Sensitivity versus grating period (P). The x-axis represents the grating period (200-500 nm), and the y -axis shows the sensitivity (nm/ RIU). The peak sensitivity occurs at $P = 300$ nm.

Table 7: Sensitivity versus Grating Period

Grating Period (P)(nm)	Sensitivity (nm/RIU)
200	22,000
250	23,500
300	25,000
350	24,500
400	23,000
450	22,000
500	21,000

To its greater performance, which makes it superior to current designs. The overall parameter variation analysis verifies the stability of the optimization process, and its comparison with state-of-the-art sensors certifies the competitiveness of the design. Other plasmonic materials or additional optimized grating parameters are potential candidates for investigation in future research in an attempt to push sensitivity over $25{,}000\ \mathrm{nm/RIU}$ and yet keep resolution.

Table 8: Comparison with State-of-the-Art PCF-Based Plasmonic Sensors

Reference	Sensitivity (nm/RIU)	Resolution (RIU)	FoM (RIU^{-1})	RI Range	Special Features
This Work	25,000	4×10^{-7}	2,500	1.33-1.40	Spiral lattice, elliptical air holes, gold grating
Zeng et al (2020)	12,600	7.94×10^{-7}	Not specified	1.15-1.36	D-shaped PCF, two nanogold belts
Yan et al (2026)	18,000.5	Not specified	Not specified	1.47-1.52	V-shaped PCF, high linearity
Liu et al (2020)	35,000	Not specified	1,120.73	1.26-1.38	ITO coating, outer surface
Xue et al (2023)	18,612	4.16×10^{-6}	Not specified	1.33-1.395	Graphene-coated grating
Hajiani et al (2024)	1,800	Not specified	268	1.39-1.45	Silver-phosphorene nanoribbons

4. Discussion and Conclusion

This paper presents a new wavelength-sensitive ultra-high refractive index resolution photonic crystal fiber (PCF)-based plasmonic sensor optimized with a wavelength sensitivity of $28{,}000\ \mathrm{nm/RIU}$ and resolution of 3.57×10^{-7} RIU through accurate geometrical parameter optimization. A D-shaped structure based on elliptical air holes and 45 nm gold coating is utilized for the design, utilizing the Finite Element Method (FEM) and an optimization approach step by step in a systematic manner. Here, these outcomes are compared to selected papers in the literature in terms of optimization techniques, solved results, and geometrical parameters' role.

The optimization technique utilized in this case uses FEM, a common technique employed by Mahfuz et al. (2019) and Rifat et al. (2015) to simulate geometries that are intricate and forecast sensor performance without requiring large-scale prototyping. Unlike one-parameter tuning in Li et al. (2018), where the gold thickness was tuned independently to reach an optimal value of 40-50"" "nm, our method optimizes over more than one parameter at a time in lattice pitch, gold thickness, and also in parallel-air hole ellipticity. It is computationally expensive but results in a complete design consistent with the recent trend towards complete optimization reflected in publications. But it is contrasted with the more explicit, sequential design of Yan et al. (2021), as to reflect a balance between computational complexity and design accuracy.

The achieved resolution of 3.57×10^{-7} RIU positions this sensor among very highresolution designs, surpassing the 4.01×10^{-6} RIU reported by Li et al. (2023) for an arc-shaped PCF with $24{,}900$ nm/RIU sensitivity. It also outperforms the dual-core design of Hussain et al. (2023), which achieved 4.12×10^{-6} RIU with $24{,}300$ nm/ RIU sensitivity. However, our resolution falls short of the ultra-high 8.13×10^{-8} RIU reported by Mahfuz et al. (2024), whose design boasts an extraordinary $123{,}000$ nm/ RIU sensitivity. This discrepancy highlights a key difference: while Mahfuz et al. prioritize extreme sensitivity, our design balances sensitivity with a high figure of merit (FOM), ensuring practical detection through sharper resonance peaks - a strategy resonant with Li et al.'s (2023) multi-metric optimization emphasis.

Geometrical parameters significantly dictate performance, a relationship well-documented in the literature. Our optimal gold thickness of 45 nm aligns precisely with the 44-45 nm range identified by Kazempour & Vahed (2020) for a D-shaped PCF, which achieved $2{,}506$ nm/ RIU sensitivity and 1.25×10^{-5} RIU resolution. This consistency underscores gold thickness as a critical factor affecting confinement loss and FWHM, as noted by Chao et al. (2022). The use of elliptical air holes further enhances performance, echoing Chao et al.'s findings that elliptical configurations outperform circular ones, achieving up to $116{,}500$ nm/ RIU sensitivity and 8.58×10^{-7} RIU resolution. Our design's D-shaped structure, enhancing evanescent field interaction, parallels Pan et al.'s (2022) approach, though our higher sensitivity ($28{,}000$ nm/ RIU vs. $5{,}626.86$ nm/ RIU) suggests superior optimization of air hole arrangement and pitch.

Material choice is also consistent with established trends. Chemical stability of gold, favored in our work and by Hassan et al. (2024), is opposed to silver-based designs like Hussain et al. (2023), which require TiO_2 coating to resist oxidation. While such hybrid approaches may enhance sensitivity, our results indicate that structural optimization alone can offer competitive performance, with no additional fabrication complexity.

In general, this paper innovates PCF-based plasmonic sensing by maximizing a D-shaped design with elliptical air holes and a 45 nm gold layer, where the achieved resolution is 3.57×10^{-7} RIU with sensitivity of $8{,}000$ nm/ RIU. The obtained results, similar to highly high-resolution designs, confirm the effectiveness of multi-parameter optimization and structural innovation. Though falling short of ultra-high values of Mahfuz et al. (2024), the optimally balanced performance figures of the design indicate pragmatic usefulness in precision sensing devices, e.g., environmental monitoring. Future studies can explore experimental proof or other lattice configurations and structures to enhance resolution even further, and continue the field's pursuit of ultra-high utility and sensitivity.

References

Cai, G., Li, W., Chen, Y., Liu, N., Song, Z., & Liu, Q. H. (2016). Modeling and design of a plasmonic sensor for high sensing performance and clear registration. IEEE Photonics Journal, 8(1), 1-11.

Chao, C.-T. C., Kooh, M. R. R., Chau, Y.-F. C., & Thotagamuge, R. (2022). Susceptible plasmonic photonic crystal fiber sensor with elliptical air holes and external-flat gold-coated surface. Photonics,

Danlard, I., & Akowuah, E. K. (2021). Design and theoretical analysis of a dual-polarized quasi D-shaped plasmonic PCF microsensor for back-to-back measurement of refractive index and temperature. *IEEE Sensors Journal*, *21*(8), 9860-9868.

Danlard, I., Mensah, I. O., & Akowuah, E. K. (2022). Design and numerical analysis of a fractal cladding PCF-based plasmonic sensor for refractive index, temperature, and magnetic field. *Optik*, *258*, 168893.

Das, S., & Singh, V. K. (2022). Highly sensitive PCF based plasmonic biosensor for hemoglobin concentration detection. *Photonics and Nanostructures-Fundamentals and Applications*, *51*, 101040.

Hajiani, T., Shirkani, H., & Sadeghi, Z. (2024). Surface plasmon resonance photonic crystal fiber biosensor: Utilizing silver-phosphorene nanoribbons for Near-IR detection. *Optics Communications*, *569*, 130801.

Hameed, M. F. O., Alrayk, Y. K., & Obayya, S. (2016). Self-calibration highly sensitive photonic crystal fiber biosensor. IEEE Photonics Journal, 8(3), 1-12.

Hassan, P., Vahid, S., Hana, S., Zahra, R., & Jamileh, H. (2024). Sensitivity enhancement in D-shaped photonic crystal fiber sensors: gold versus silver plasmonic layers. Plasmonics, 1-8.

Hussain, N., Masuk, M. R., Hossain, M. F., & Kouzani, A. Z. (2023). Dual core photonic crystal fiber based plasmonic refractive index sensor with ultra-wide detection range. Optics Express, 31(16), 26910-26922.

Johnson, P. B., & Christy, R. W. (1972). Optical constants of the noble metals. *Physical review B*, *6*(12), 4370.

Kazempour, M. V., & Vahed, H. (2020). Plasmonic D-shaped photonic crystal fiber biosensor with gold layer for sensing of the refractive index. International Journal of Optics and Photonics, 14(2), 209-216.

Li, H. P., Ruan, J., Li, X., Zhang, Q. Q., Chen, J. J., He, T., & Wei, G. (2023). High-sensitivity refractive index sensor of arc-shape photonic crystal fiber based on surface plasmon resonance. Progr. Electromagn. Res. C, 137, 29-38.

Li, X., Li, S., Yan, X., Sun, D., Liu, Z., & Cheng, T. (2018). High sensitivity photonic crystal fiber refractive index sensor with gold coated externally based on surface plasmon resonance. Micromachines, 9(12), 640.

Liu, Q., Sun, J., Sun, Y., Ren, Z., Liu, C., Lv, J., ... & Chu, P. K. (2020). Surface plasmon resonance sensor based on photonic crystal fiber with indium tin oxide film. *Optical Materials*, *102*, 109800.

Mahfuz, M. A., Afroj, S., Hossain, M. A., Hossain, M. A., Rahman, A., & Habib, M. S. (2024). An ultra-sensitive visible-ir range fiber based plasmonic refractive index sensor. arXiv preprint arXiv:2401.10968.

Mahfuz, M. A., Hossain, M. A., Haque, E., Hai, N. H., Namihira, Y., & Ahmed, F. (2019). A bimetallic-coated, low propagation loss, photonic crystal fiber based plasmonic refractive index sensor. Sensors, 19(17), 3794.

Mohammadd, N., Amin, R., Ahmed, K., & Bui, F. M. (2023). Plasmonic Nanomaterials in Sensors. *Biosensors Nanotechnology*, 185-200.

Pan, H., Pan, F., Zhanga, A., Cao, C., & Xue, F. (2022). Wide refractive index detection range surface plasmon resonance sensor based on D-shaped photonic crystal fiber. Optical and Quantum Electronics, 54(6), 393.

Rifat, A. A., Mahdiraji, G. A., Chow, D. M., Shee, Y. G., Ahmed, R., & Adikan, F. R. M. (2015). Photonic crystal fiber-based surface plasmon resonance sensor with selective analyte channels and graphene-silver deposited core. Sensors, 15(5), 11499-11510.

Vieira, R. A., & Rodriguez-Esquerre, V. F. (2022). High sensitivity D-shaped photonic crystal fiber plasmonic refractive index sensor. Optical Fibers and Sensors for Medical Diagnostics, Treatment and Environmental Applications XXII.

Xue, F., Yao, Y., Xu, P., Luo, J., Li, L., Zhang, L., & Liu, E. (2023). Ultra-high sensitive refractive index sensor based on D-shaped photonic crystal fiber with graphene-coated Ag-grating. *Heliyon*, *9*(4).

Yan, X., Fu, R., Cheng, T., & Li, S. (2021). A highly sensitive refractive index sensor based on a V-shaped photonic crystal fiber with a high refractive index range. *Sensors*, *21*(11), 3782.

Zeng, W., Wang, Q., & Xu, L. (2020). Plasmonic refractive index sensor based on D-shaped photonic crystal fiber for wider range of refractive index detection. *Optik*, *223*, 165463.